JOURNAL OF MATERIALS SCIENCE 26 (1991) 3463–3476

Formation of silicon carbide whiskers and their microstructure

A. CHRYSANTHOU*, P. GRIEVESON
Department of Materials, Imperial College of Science and Technology, London, UK
A. JHA
Department of Materials Technology, Brunel University, Uxbridge, Middlesex UB8 3PH, UK

Thermodynamic and kinetic conditions for the formation of SiC whiskers are established. The mechanism of their nucleation and growth are studied and, on this basis, the magnitude of the thermally activated barrier is determined from the rate of reduction data. The microstructures of whiskers are analysed and the role of interfacial tension between the nuclei and impurities, and the metallic iron catalyst is studied in relation to the formation of SiC whiskers. A possible reason for polytypism in SiC whiskers is also proposed.

1. Introduction

Silicon carbide is a commonly used ceramic material with attractive properties such as high strength, stiffness, good wear and corrosion resistance, some of which are characteristics of a typical covalently bonded material. The atomic arrangement of β-SiC is based on a tetragonal grouping of C atoms, as in the structure of diamond, surrounding a silicon atom in the centre with parallel layers of tetrahedra situated perpendicular to the trigonal axis of the cube. The hexagonal α-SiC modification is related to the cubic arrangement by rotation of the tetrahedra in alternate sheets so that they lie in parallel or anti-parallel orientations. The α-form exhibits polytypism due to different stacking arrangements of Si and C. A number of polytypes of α-SiC have been reported by various workers [1–8]. One of the reasons for the occurrence of various polytypes is believed to be due to the impurities, such as oxygen [8–10]. Oxygen can participate in the growth process of SiC crystals and such illustrations on the role of O_2 impurities during the growth process are cited elsewhere [8, 9]. The mechanism of $\beta \rightarrow \alpha$ phase transformation in SiC under ceramic fabrication conditions has been observed and studied by several workers [7, 9, 11–14] and it has been concluded that the reaction sintered (RS) and chemically vapour deposited (CVD) SiC predominantly consist of the β-form. A small volume fraction of the α-form is always present under these processing conditions.

Silicon carbide whiskers and fibres have recently attracted enormous interest because of their useful mechanical properties at high temperatures. This has led to the processing of SiC whiskers and fibres as reinforcement materials in metal and ceramic matrix composites. SiC fibres are being currently processed from carbosilane polymers [15]; whereas the whiskers of β-SiC are produced by CVD and reduction techniques using different types of starting materials [16–19]. The role of impurities during the growth process was particularly examined by a few workers [17, 18] and their presence is still thought to be important to explain the mechanism of whisker growth. Impurities have also been known to aid the growth of other kinds of whiskers.

An interestingly unique approach has been taken by Wada *et al.* [20] to grow whiskers of silicon carbide. In this work, a systematic study has been carried out by signifying the phase equilibria in the Si–C–O system and relevant phase boundaries have been constructed. During the present work, the formation of SiC whiskers has been studied by reducing various forms of Si with C under different partial pressures of CO gas. The effect of temperature and role of SiO gas pressure on the production of SiC whiskers is discussed, together with a model for nucleation and growth. On the basis of physico-chemical parameters, the phase transformation in SiC ($\beta \rightarrow \alpha$) whiskers is also explained signifying its role while processing this material as reinforcement in metal or ceramic matrices.

2. Experimental procedure

Three different kinds of SiO_2 were used as the starting material to investigate the effect of topology and surface area of oxide particles on the reaction rate. These were crushed quartz (99.98% pure), precipitated silica (99.98% pure) which is an ultra-fine material and crushed gel silica glass (99.9% pure); the latter having the largest surface area of the three. Prior to its use, gel silica was dried at 300 °C for 36 h in a flowing stream of dry air. This was to ensure that the material was free from any carbon oxidant such as moisture which at

* *Present address*: Department of Materials Engineering and Materials Design, Nottingham University, University Park, Nottingham NG7 2RD, UK.

0022–2461/91 $03.00 + .12

elevated temperatures may partake in the reduction of silica. Graphite and lampblack were used as reducing agents but during trial runs the former was subsequently found unsuitable. Lampblack is a type of carbon soot and has a very fine particle size which cannot be easily determined by conventional techniques. Therefore this was crudely judged to be of submicrometre size.

Appropriate amounts of precipitated silica, crushed quartz, gel powder and lamp black were weighed in stoichiometric proportions $SiO_2:C = 1:2$ ratio. The amount of C added was kept in excess of the stoichiometric value necessary to sustain the reaction $SiO_2 + 3C = SiC + 2CO$. In some mixtures, 5 wt % $FeCl_3$ was also added to investigate its role as a catalyst during the reduction of SiO_2. The weighed materials were thoroughly mixed and pelletized into cylindrical discs using a 12.25 mm steel die. The load applied during pressing was kept constant.

A diagram of the reaction apparatus is shown in Fig. 1. The main feature of this apparatus was the use of a Cartesian manostat (A) which was used to control the pressure in the reaction tube (B). An arrangement of saffil insulators (C) supported by an alumina tube (D) was placed inside the silica reaction tube (B). A graphite crucible (E), which also acted as a heat susceptor rested inside the insulators and it was heated rapidly using a radio frequency induction coil (F). The temperature was measured by using a Pt–6% Rh/Pt–30% Rh thermocouple (G) in contact with the bottom of the graphite crucible (E). The e.m.f. across this temperature device was measured by using a potentiometer. Having established the required temperature, the leak-proof reaction chamber was evacuated by means of a rotary pump (H). Carbon monoxide gas was then introduced into the chamber to the desired pressure; this being monitored by a mercury manometer (I). The manostat (A) was then isolated from the pump using a valve (J) and the supply of CO gas to the reaction chamber was cut-off by closing the tap (K). Prior to the evacuation process, the tap (L) was opened and it was by using this tap that the reaction chamber was maintained at the desired total reduced pressure. During reaction, if any extra volume of gas arrived in the manostat through the connecting glass tube, it depressed the mercury column. This allowed a leak to occur through the porous disc (M), which otherwise remained sealed, and the excess gas left the manostat through a one-way valve junction (N) to the buffer volume (R). For reaction to commence, the pressed-pellet was dropped into the graphite crucible using a magnet and push rod device (S). The progress of the reaction was followed by measuring the volume of the gas evolved at specific time intervals. The volume of gas was converted into percentage volume of CO evolved (% CO vol.) via the gas law relationship and the stoichiometry of the reduction reaction. These data were used to construct the rate of reduction curves for silica under different conditions. At the end of each experiment, the total loss in weight sustained by a pellet was also independently verified by weighing the reduced pellet on an analytical balance and obtaining a difference between the initial and final weights which was in good agreement with the total volume of gas evolved.

New solid crystalline phases produced during the course of silica reduction were identified by means of X-ray diffraction using a Guinier focusing camera with monochromatic CoK_α radiation. The reaction product was also examined using scanning and transmission electron microscopes, the details of which will be discussed below.

These results were analysed to understand the kinetics and mechanism of whisker growth.

3. Results and discussion

3.1. Reduction of quartz and precipitated silica with lampblack at different temperatures, T, at a given partial pressure of CO, P_{CO}

The rate of reduction curves for quartz and precipitated silica are shown in Figs 2 and 3 at various CO isobars. This is presented in terms of volume of CO evolved, vol. CO (ml) against time. The reduction rate was observed to be linearly related to log time, log t, as

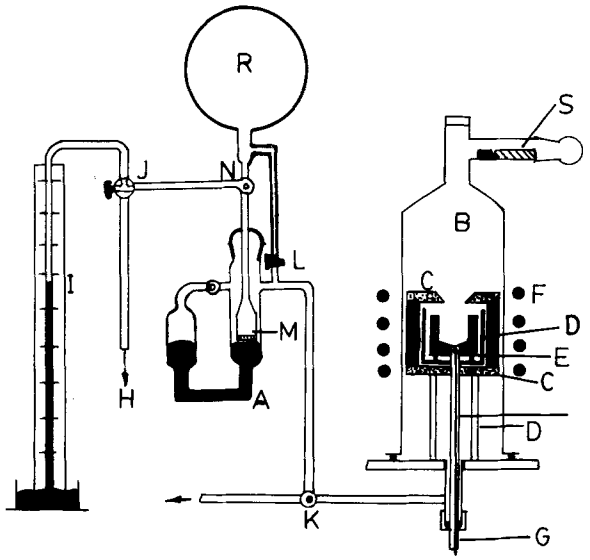

Figure 1 Schematic diagram of the apparatus.

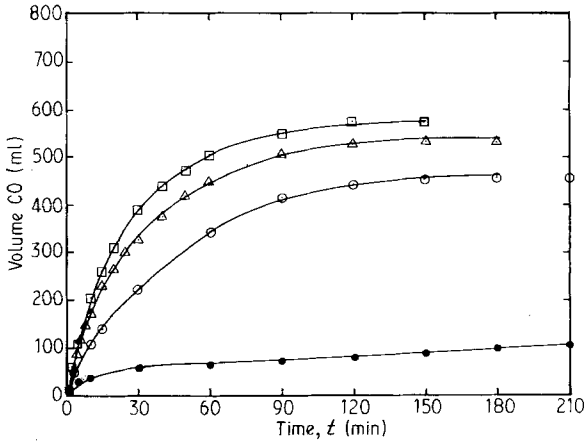

Figure 2 Rates of evolution of CO gas (ml) during the reduction of quartz at different CO partial pressures. $T = 1550\,°C$. P_{CO} (atm): (□) 0.125, (△) 0.25, (○) 0.50, (●) 1.0.

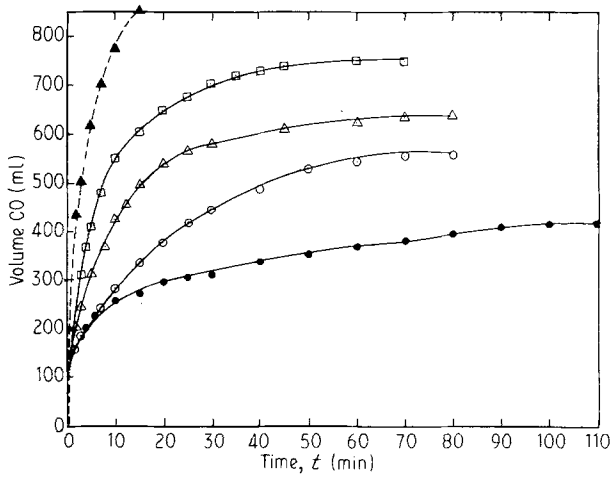

Figure 3 Rates of evolution of CO gas (ml) during the reduction of precipitated silica at different CO partial pressures. $T = 1550\,°C$. (▲) $FeCl_3$ catalyst. Other symbols as in Fig. 2.

shown in Figs 4 and 5. Both the reduction rate and the extent of reaction increases with temperature. A similar behaviour is observed when the total pressure is reduced as expected from the Le Chatelier principle which indicates that if during a reaction the partial pressure of the product gas is reduced, the equilibrium shifts to the right. The slope of vol % CO evolved versus log t curve was measured at various temperatures and a given P_{CO} to construct an Arrhenius plot for each type of silica used. This relationship is shown in Fig. 6. The gradient of the Arrhenian line indicates that the apparent activation energy, E_a, for the reduction process is considerably smaller than the value reported by Lee and Cutler [18]. In the present investigation, the value of E_a at each isobar is roughly 100 kJ mol^{-1} SiC which is four to five times less than that derived elsewhere [18]. This difference is due to the type of C used. Lampblack has a very high surface area and reactivity compared to other forms of C. Turkdogan and Vinters [21] have studied the reactivity of various forms of C and have shown that the rate of oxidation and the value of E_a depends upon the C type used. A comparison of rate of reduction data is shown in Fig. 7 from which it is evident that the type of C, in this case lampblack, had a pronounced effect in determining the speed of chemical reaction. A limited number of experiments was carried out using $FeCl_3$ as a catalyst for the carbon oxidation reaction. Its presence increased the rate of reduction as shown in Fig. 3. Also, when crushed gel silica was used as the starting material, the rate of reduction was much faster than with the precipitated silica or crushed quartz at a given temperature and CO partial pressure. The catalytic effect thus appears to compete with the effective reaction surface area of the type of silica used.

From these sets of results, the following two conclusions were deduced:

(i) the rate of reaction depends upon the effective surface area of silica particles;

(ii) the rate of carbon oxidation can be substantially altered by the addition of a catalyst, such as $FeCl_3$, or by the choice of a type of C, for example the lampblack being one of the most reactive carbons (cf. graphite).

3.2. Verification of formation of SiC whiskers

Reduced samples were examined by scanning electron microscopy to verify the formation of SiC whiskers. There were experimental conditions where significant reduction of silica had occurred but no whiskers were observed as seen in the case of reduction with $FeCl_3$. The average volume fraction of whiskers in a given sample was determined by quantitative optical microscopy and statistical analysis. In Fig. 8 the rate of reduction is plotted against $1/T$ at various CO isobars and each point on this plot signifies the volume per cent of SiC whiskers in the pellet designated by the

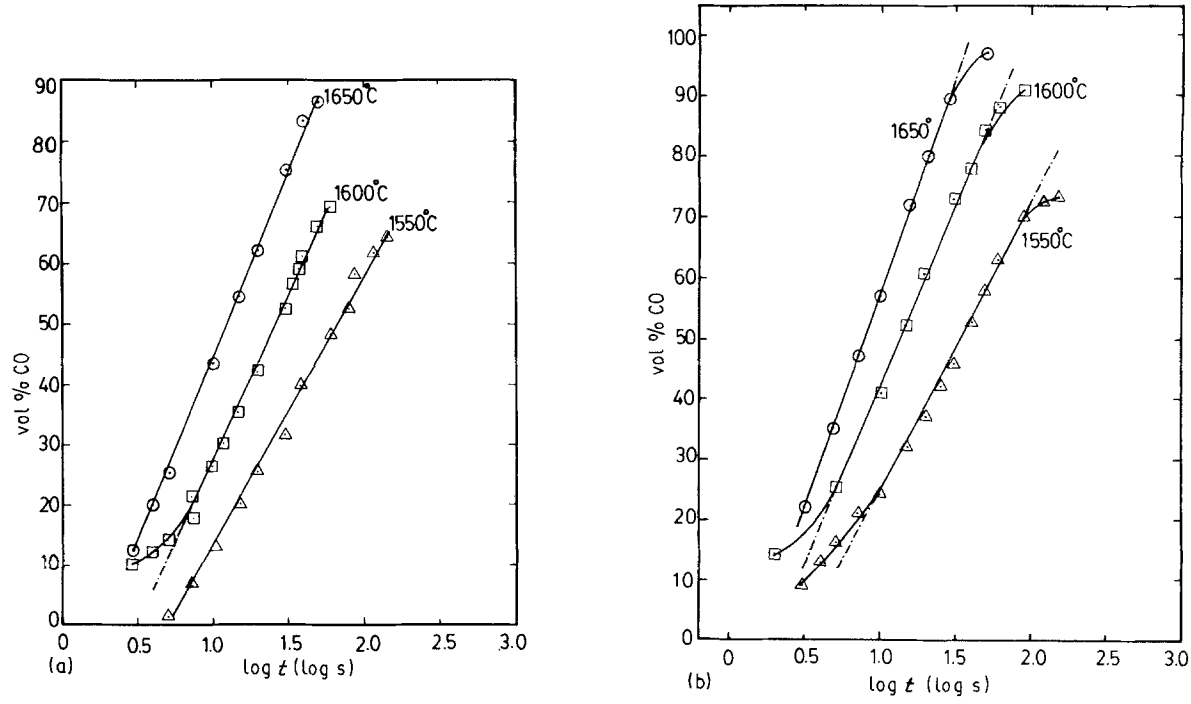

Figure 4 Per cent CO vol. evolved versus log t curves for quartz at different temperatures. (a) $P_{CO} = 0.50$ atm, (b) $P_{CO} = 0.25$ atm.

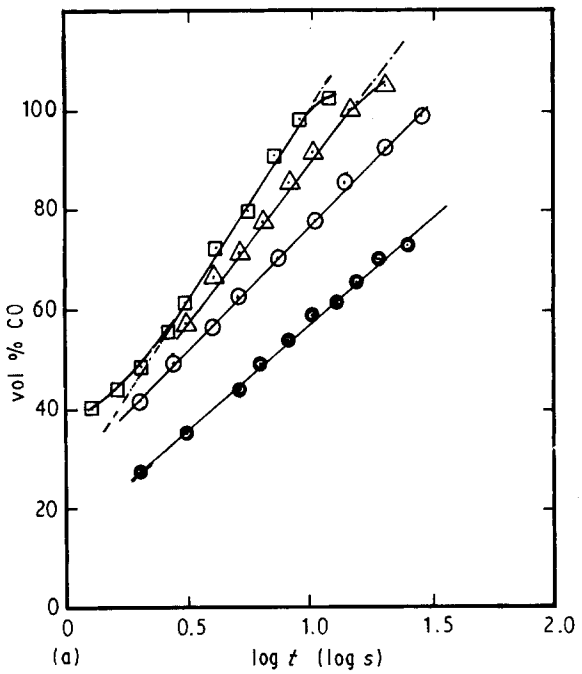

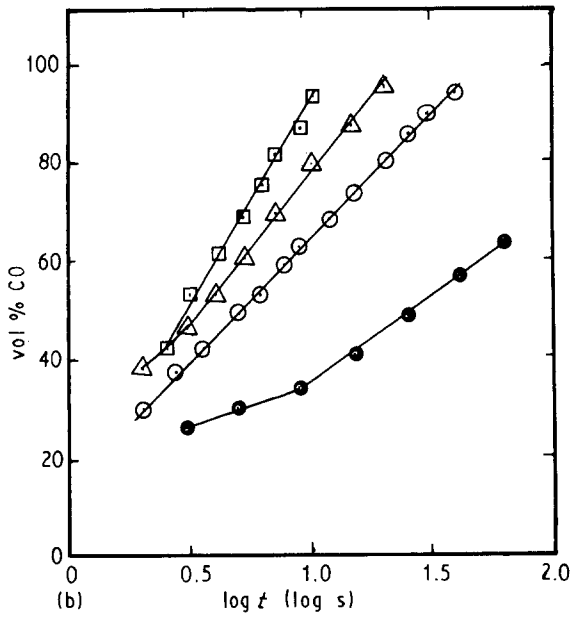

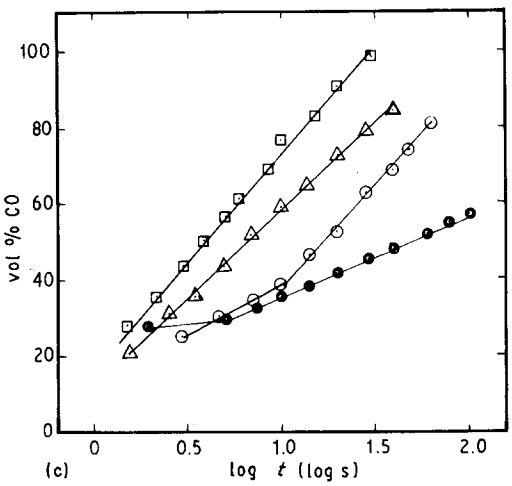

Figure 5 Per cent CO vol. evolved versus log t curves for precipitated silica at different temperatures. (a) 1650 °C, (b) 1600 °C, (c) 1550 °C. For key, see Fig. 2.

number within small parentheses. The data points at each CO partial pressure are joined for the reduction of precipitated silica. From this plot, the factors controlling the formation of whiskers are summarized below:

(i) whiskers do not form at very "high temperatures and low CO partial pressures";

(ii) their volume fraction in the reduced pellet significantly drops at "high CO pressure and low temperatures"; thus indicating an intermediate temperature and pressure range for a high product yield.

In addition to these, any other factors which indirectly affect the partial pressures of the significant gaseous species either in the reaction chamber or within the pellet can influence whisker yield. For example, $FeCl_3$ catalyses the Boudouard reaction ($C + CO_2 = 2CO$) which at a low total CO pressure ($P_{CO} = 0.125$ atm) does not yield any SiC whiskers. The catalytic effect aids whisker formation only at intermediate CO pressures. The significance of operating variables are described below by understanding the physical chemistry of the reduction reaction.

3.3. Physical chemistry of the Si–C–O system

At high temperatures (above 1300 °C) SiO_2 decomposes to SiO and oxygen gas according to the reaction $SiO_2(s, l) = SiO(g) + \frac{1}{2}O_2(g)$. In the presence of carbon this reaction becomes thermodynamically more favourable because the chemical potential of O_2 gas produced is reduced by forming a thermodynamically stable gas CO, which means the gaseous decomposition of silica in the presence of carbon is a two-stage reaction as shown below

$$SiO_2(l, s) = SiO(g) + \tfrac{1}{2}O_2(g) \quad (1)$$

$$C(gr) + \tfrac{1}{2}O_2(g) = CO(g) \quad (2)$$

Adding Equations 1 and 2 yields

$$SiO_2(l, s) + C(gr) = SiO(g) + CO(g) \quad (3)$$

Here graphite (gr) is chosen as the standard state for carbon.

The formation of SiC by the carbothermic reduction of SiO_2 is governed by two different mechanisms of reaction. In the beginning, when each SiO_2 particle is in contact with carbon, the reduction process is either a purely solid–solid or a liquid–solid (above 1450 °C, quartz melts). The SiO gas is subsequently reduced by carbon to produce SiC and CO gas

$$SiO(g) + 2C(gr) = SiC(s) + CO(g) \quad (4)$$

When the initial period has elapsed, the reacting particles lose physical contact with each other, although above 1450 °C, Reaction 3 may continue due to the presence of liquid quartz. In subsequent stages, when the pressure of CO becomes significant within the pellet, it reacts with liquid or solid SiO_2 to yield SiO and CO_2 gases, via the reaction

$$SiO_2(l \text{ or } s) + CO(g) = SiO(g) + CO_2(g) \quad (5)$$

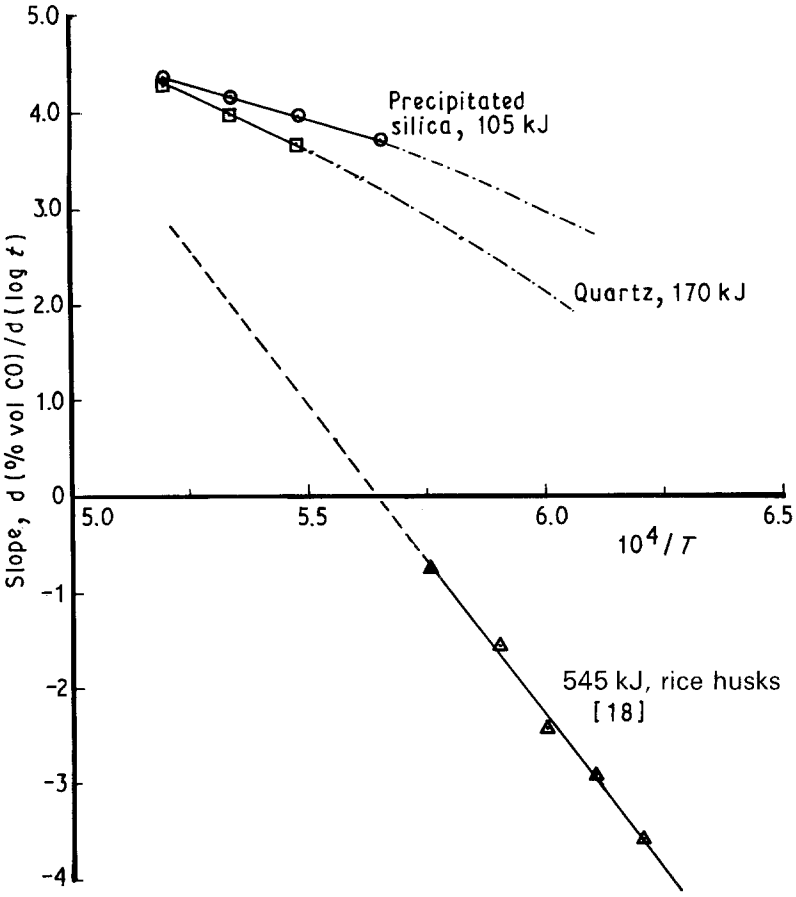

Figure 6 Arrhenius plots (slope vol % s^{-1} CO versus $1/T$) for the rates of reduction of quartz and precipitated silica. The results are also compared with those of Lee and Cutler [18].

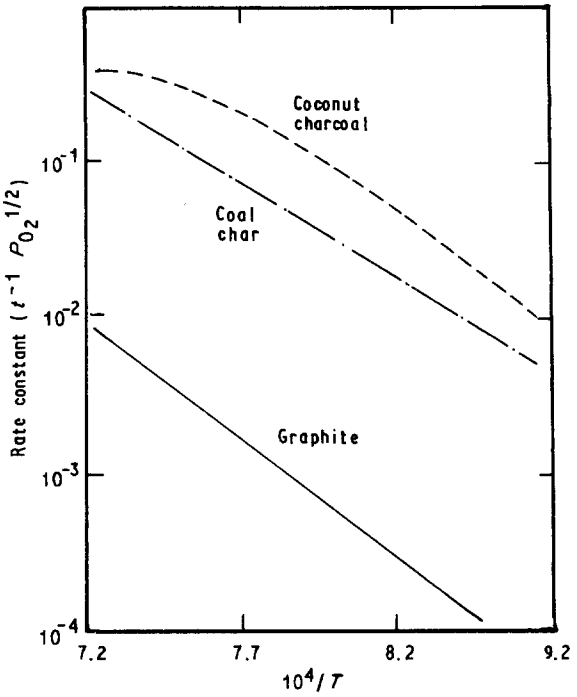

Figure 7 Comparison of rates of oxidation of various forms of C [21].

which leads to the gaseous reduction of SiO by CO gas

$$SiO(g) + 3CO(g) = SiC + 2CO_2(g) \quad (6)$$

Any CO_2, which is produced is expected to be consumed immediately by the surrounding C particles to yield CO via the Boudouard reaction. The value of the standard Gibbs free energy change, ΔG^0 (J mol^{-1}) along with the derived values of the equilibrium constants for each Reaction 1–6 are listed in Table I. Based on these ΔG^0 values for Reactions 3 and 4, a relationship to show the dependence of P_{SiO} on P_{CO} was constructed for each temperature isotherm in Fig. 9.

In Reaction 3, at equilibrium P_{CO} is inversely proportional to P_{SiO} whereas in Reaction 4 the CO pressure rises with SiO partial pressure and is in equilibrium with SiO(g), C and SiC phases.

In order to establish the relationship shown in Fig. 9, the following equations were derived

$$K_3 = \exp\left(-\frac{\Delta G_3^0}{RT}\right) = (P_{SiO} \cdot P_{CO}) \quad (7)$$

and

$$K_4 = \exp\left(-\frac{\Delta G_4^0}{RT}\right) = \frac{P_{CO}}{P_{SiO}} \quad (8)$$

This interrelation between P_{CO} and P_{SiO} indicates that the cross-over points (a, b, c, d) signify the phase invariance at each temperature where the three phases SiC–SiO_2–(SiO + CO) are in equilibrium. From these curves, it is evident that the reaction SiO_2(l, s) + 3C(gr) = SiC(s) + 2CO(g) is a combination of Reactions 3 and 4, where each of these play an important role in the characterization of the mechanism of overall reaction. For the formation of SiO gas, the reduction of the CO pressure is an essential requirement without which the synthesis of SiC via Reaction 4 is impossible (alternatively a reduction in CO_2 pressure

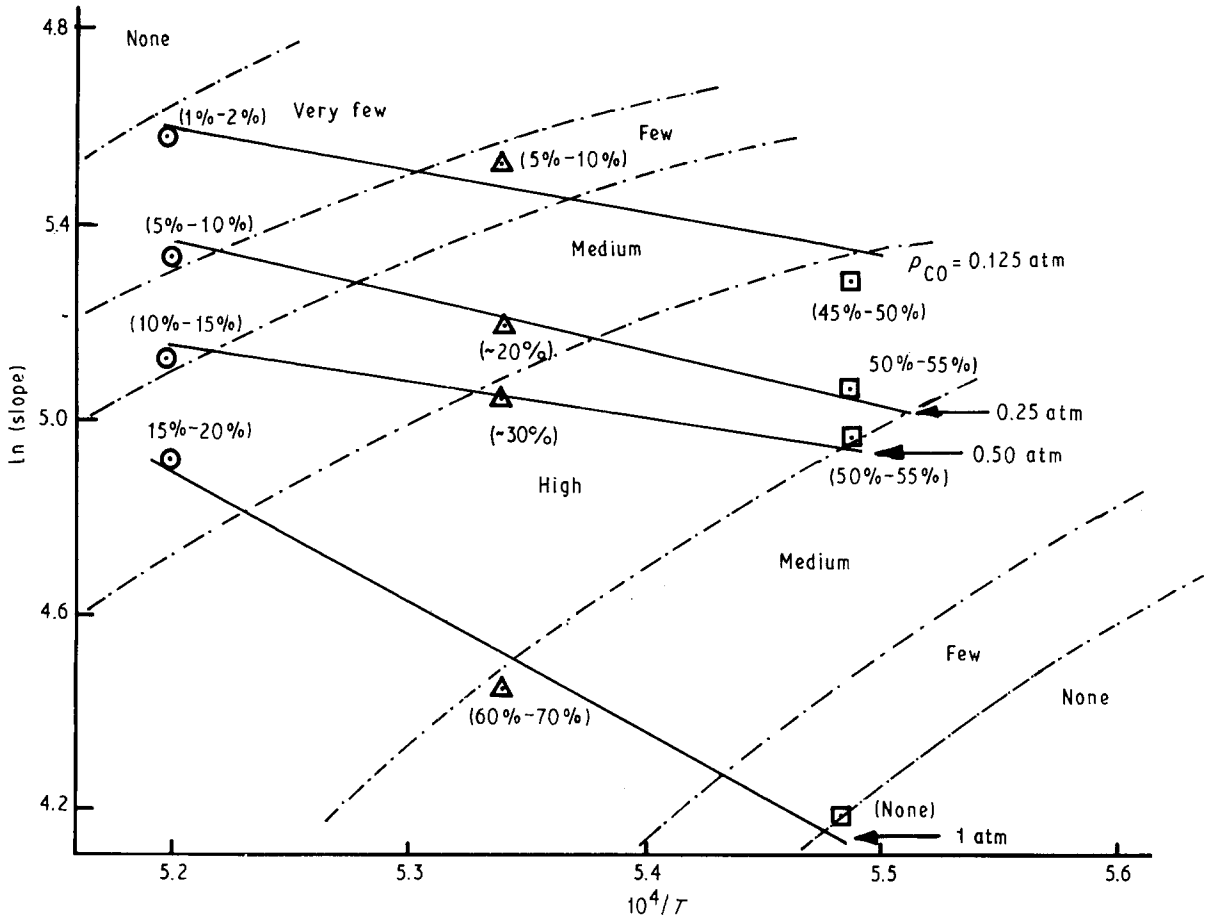

Figure 8 Rates of CO evolution (slopes of linear regime in Fig. 5) versus $1/T$ curves at different CO isobars for the reduction of precipitated silica. The values within the brackets are the percentage yield of SiC whiskers. (⊙) 1650 °C, (△) 1600 °C, (⊡) 1550 °C.

TABLE I The calculated values for the standard Gibbs free energy change, ΔG^0, and equilibrium constants, K, in the Si–O–C system

Reaction	$\Delta G^0 = \Delta H^0 - T\Delta S^0$ (J mol^{-1})	K_{1550}	K_{1600}	K_{1650}
1. $\{SiO_2\} = (SiO) + \frac{1}{2}(O_2)$	802 718–258.2T	3.06×10^{-10}	1.3×10^{-9}	4.8×10^{-9}
2. $\langle C\rangle + \frac{1}{2}(O_2) = (CO)$	− 114 363 − 85.7T	5.67×10^{7}	4.6×10^{7}	3.8×10^{7}
3. $\{SiO_2\} + \langle C\rangle = (SiO) + (CO)$	688 354–344T	0.017	0.058	0.185
4. $(SiO) + 2\langle C\rangle = \langle SiC\rangle + (CO)$	− 132 770 + 33.9T	110	87.1	69.8
5. $\{SiO_2\} + (CO) = (SiO) + (CO_2)$	514 258–176.5T	3.05×10^{-6}	7.5×10^{-6}	1.78×10^{-8}
6. $(SiO) + 3(CO) = \langle SiC\rangle + 2(CO_2)$	− 465 568 + 379T	3.5×10^{-7}	1.5×10^{-7}	7.1×10^{-8}
7. $\langle C\rangle + (CO_2) = 2(CO)$	167 738 − 172.T	1.5×10^{4}	2.02×10^{4}	2.7×10^{4}

( ) Gas phase, $\langle\ \rangle$ solid phase, $\{\ \}$ liquid phase.

is required if CO is considered to be the reducing gas) because the removal of CO from the reaction chamber is essential to shift the equilibrium of Reaction 4 to the right. This signifies that a reduction in CO pressure is the only equilibrium thermodynamic requirement for the synthesis of SiC as it is both necessary as well as a sufficient condition. The percentage yield of SiC under specific operational conditions from Fig. 8 is superimposed on Fig. 9 and these points are joined together to form a curve, e.g. (xy, rs and pq). These curves evidently lie in the region where the SiO pressure is high and the CO pressure is low but the magnitude of the CO and SiO pressures derived from the experimental data indicates that the SiO pressure required should be more than the estimated equilibrium values. This is clearly an indication of a kinetic requirement for the synthesis of SiC crystals; which follows the Le Chatelier principle. However, it must be emphasized that if CO pressure is reduced to a value much more than is kinetically necessary, this causes extreme volatilization of SiO and under such conditions there is not enough reduction potential available in the gas phase that would be able to sustain the formation of SiC. No whisker growth was observed at moderately low pressures of CO.

The curve for per cent yield of SiC for whisker growth shown in Fig. 8 indicates that at each CO isobar, the maximum yield coincides with the corresponding high SiO pressure, e.g. for $P_{CO} \approx P_T = 0.25$ atm at 1600 °C, P_{SiO} equals 0.235 atm which is higher than the invariant point "b" in Fig. 9. This is in agreement with the above statement.

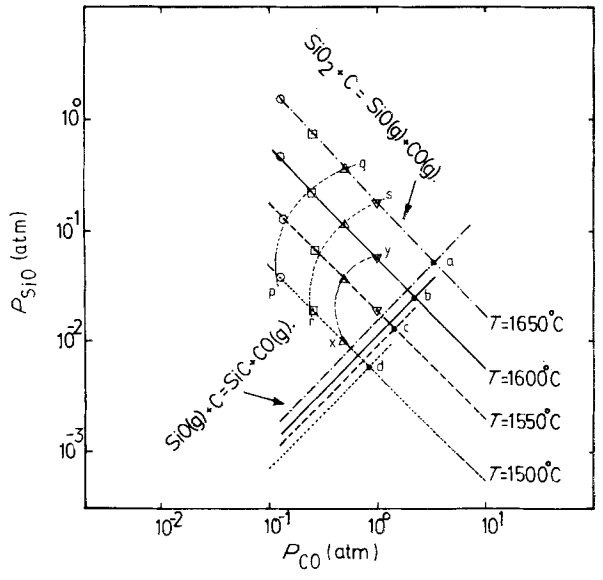

Figure 9 P_{SiO} versus P_{CO} diagrams at different isotherms for the condition of whisker growth. The cross-over points a, b, c and d designate the condition of phase invariance determined at the temperatures indicated. pq, rs and xy are the regions of high whisker yield. P_{CO} (atm): (⊙) 0.125, (⊡) 0.25, (△) 0.50, (▽) 1.0.

3.4. Role of catalyst and iron impurities

The rate of carbothermic reduction of oxides is determined by the rate of CO gas evolution via the Boudouard reaction, i.e. $C(gr) + CO_2(g) = 2CO(g)$. The gasification of C by CO_2 also relies on the catalytic mechanism. The donation of electrons to a carbon ring in the graphitic structure during catalytic oxidation is the most accepted theory [22], according to which, transition and alkali metals donate one of their outermost electrons to the C–C bond in the ring. This electronic exchange is also believed to occur when their compounds such as chlorides and carbonates are used as catalysts [22]. This charge transfer causes a rise in the potential energy of the ring structure and in the presence of O_2, a lower energy state is acquired by the adsorption of an O_2 atom, thus forming a $(CO)^-$ bond which is much weaker than the C–C bond. This is believed to be the most important step in the oxidation of C. Turkdogan and Vinters [23] have used the reaction rate theory and determined the energetics of the process of (CO)* activated complex formation. The charge donation process thus necessitates the catalytic oxidation of C. By adding $FeCl_3$ during the reduction of silica, the decomposition of $FeCl_3$ to Fe and Cl_2 gas takes place above 800 °C [24]. Metallic iron, thus produced, participates in the catalytic reaction. The electron donation is facilitated which is summarized as

$$\text{C} + e^- = \text{C}^- \quad (9)$$

$$\text{C}^- + [O]_{ad} = (CO)^- = (CO) + e^- \quad (10)$$

Here the suffix "ad" designates the adsorbed oxygen. In the case of transition metals such as Fe, $Fe^{2+} \rightarrow Fe^{3+}$ (3d → 4S) transition occurs whereas alkali metals acquire a 1^+ valence state after donating their outermost electron. The above mechanism of catalysis also underlines the principle of catalytic oxidation based on the molecular adsorption of O_2 on the C surface because the adsorption of a gas on a solid substrate is a physico-chemical phenomenon which also depends upon the exchange of electronic charge between the substrate and the adsorbent.

Lampblack is an active form of C which has a very large surface area and potentially large number of sites for oxygen adsorption. There are fewer such sites available in graphitic C and they can only be created by the addition of a catalyst. The reasoning illustrated above explains why a C fibre, whose surface is invariably contaminated with sodium (originating from the processing of the fibre) undergoes rapid oxidation above 500 °C in air whereas a lump of pure graphite does not even begin to burn above 800 °C. Other forms of impurities can also induce such a charge exchange and accelerate the oxidation of C. This points out that as the surface area of carbon increases this is tantamount to having a larger number of unsaturated C–C bonds in the structure of lampblack than in graphite. The presence of these sites thus depends upon the structure of carbon under consideration and the impurities (such as transition or alkali metals) present.

3.5. Nucleation of whiskers on impurities

The micrographs in Figs 10 and 11 indicate that whisker nucleation can occur on impurities such as iron (which was present as a catalyst) and carbon, respectively. The spherulitic shapes observed in the micrographs are the frozen droplets of Fe–Si–C liquid containing 25 at % Si. This is not surprising as there has been evidence in the literature [25–27] that a C saturated Fe–Si liquid alloy can exist below 1250 °C. Bootsma *et al.* [28] have pointed out that the alloy composition could be a eutectic liquid having an invariant temperature at around 1200 °C.

In Fig. 12 the calculated liquidus curve in a FeSi–SiC pseudo binary system has been drawn and from this phase diagram, the estimated eutectic temperature is at 1165 °C. The liquid composition of 35 at % Si is slightly higher than the values reported by Bootsma *et al.* [28]. Here these liquidus curves are obtained from the relationship $\Delta\bar{G}_i = RT \ln X_i = \Delta S_m(T - T_m)$ relationship where X_i is the atom fraction of ith component in the liquid alloy and ΔS_m and T_m are the entropy of fusion and the melting point, respectively. FeSi is an ordered bcc compound having a melting point of 1418 °C and an estimated ΔS_m value for this intermetallic phase is 5 e.u. (1 e.u. = 4.2 J K^{-1} mol^{-1}) whereas SiC is a compound which melts incongruently at 2700 °C [29]. It has been assumed that SiC, which has a diamond cubic structure, upon liquefaction produces an entropy change equal to 2 e.u.

The formation of metal droplets during isothermal reduction of SiO_2 is a combination of two reactions at elevated temperature. The first reaction refers to the thermal decomposition of $FeCl_3$ to Fe and Cl_2 gas as indicated in Section 3.4; the latter is readily swept away from the reaction chamber. The second reaction is the carbothermic reduction of SiO gas to metallic Si, i.e. $SiO(g) + C$ or $CO(g) = Si(l) + CO(g)$ or

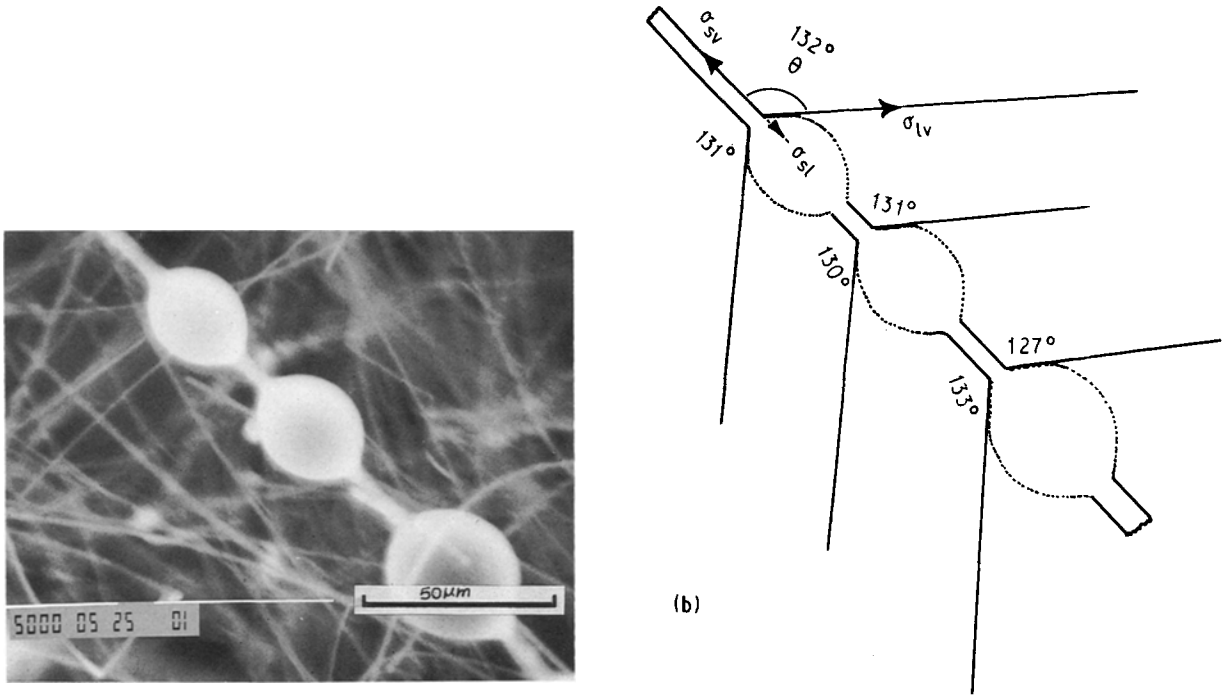

Figure 10 (a) Nucleation of SiC whiskers on Fe–Si–C alloy. (b) The schematic diagram of the "bead-necklace" morphology of SiC whisker (Fe–Si–C) alloy droplet from which the contact angles, θ, between the liquid droplet and β-SiC are determined. These are shown in this figure which averages 130°. σ_{ls}, σ_{vs} and σ_{lv} are the liquid–solid, vapour–solid and liquid–vapour interfacial tensions, respectively.

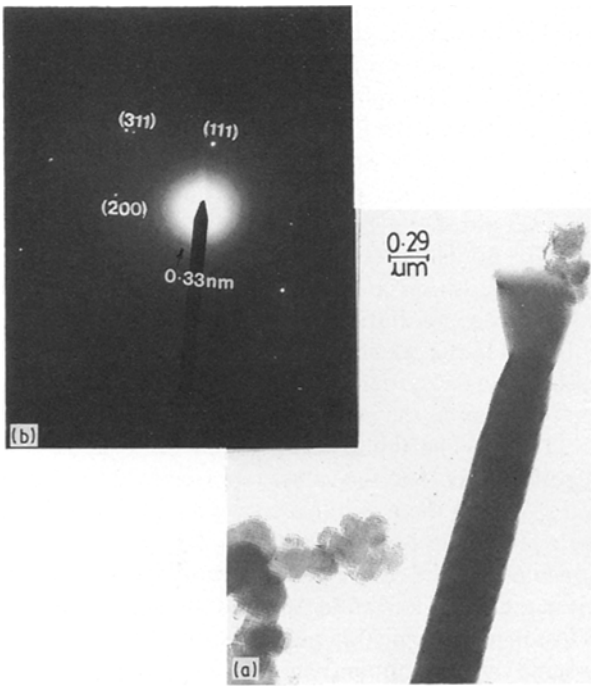

Figure 11 (a) Nucleation of SiC whiskers on C. (b) Selected-area diffraction pattern showing the ring pattern for the graphitic C and the spots designate the reciprocal lattice vectors of β-SiC.

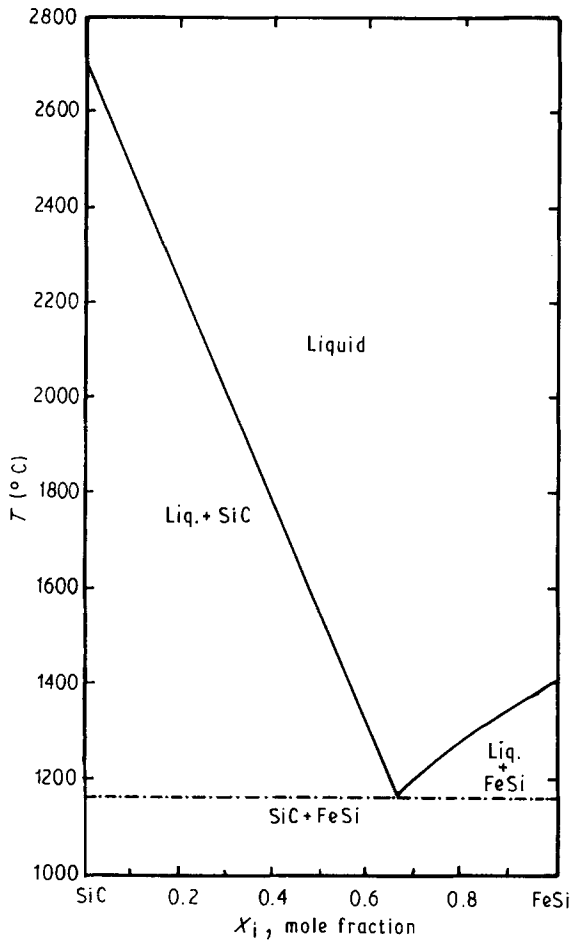

Figure 12 Calculated FeSi–CSi pseudo binary phase diagram indicating a low-temperature Fe–Si–C liquid.

CO_2(g). Metallic Si produced from the gas phase nucleates at energetically preferred sites; by means of this it lowers the chemical potential. In the presence of metallic Fe, either produced from rapid decomposition of $FeCl_3$ or added as a catalyst, these energetically favourable sites for silicon droplets are liquid Fe–C alloy. The dissolution of Si in Fe metal above 1450 °C is thermodynamically possible, and in the presence of C, the ternary Fe–Si–C liquid could also form as shown in the calculated pseudo binary section, see Fig. 12. Droplet formation, therefore, occurs well below the melting point of pure Fe (1536 °C). The dissolution of Si in liquid Fe–C alloy also reduces the

interfacial tension which energetically favours the nucleation of liquid droplets but also lowers the interfacial free energy during nucleation of subsequent SiC whisker growth. In addition to the nucleation of SiC from Fe–Si–C droplets shown in Fig. 11, whiskers also grow from C which indicates that SiO gas reduction can directly result into SiC nucleation on the C surface. These whiskers have a different morphology, see Fig. 11. The inset shows a diffused diffraction ring for C.

The process of nucleation of SiC whiskers at the specific site featured in Fig. 10 points out that the whole process is dictated by the reaction

$$\{Si\}_{Fe} + \{C\}_{Fe} = \langle SiC\rangle \qquad (11)$$

where the brace { } indicates dissolved species in Fe–Si–C alloy. The equilibrium constant for Reaction 11 is

$$K_{11} = \frac{a_{\langle SiC\rangle}}{\{a_{Si}\}\{a_C\}} = \exp\left(-\frac{\Delta G_{11}}{RT}\right) \qquad (12)$$

and is only thermodynamically feasible at temperatures above 1165 °C where $\Delta G^0 = -13\,680 + 96.5T$ J mol^{-1} SiC. In Equation 12, a_{Si} and a_C are fixed at a given T and total pressure by the Gibbs phase rule for Fe–Si–C–O equilibrium; the equilibrium phases being SiC, Fe–Si–C alloy, C and the gas mixture. The combination of the metallization and the reduction reaction of SiO gas fixes the composition of the alloy phase for a given P_{CO} value and temperature. Evidently for SiC to form, a_{SiC} must be at least equal to 1, then for the nucleation of SiC from Equation 12

$$\{a_{Si}\} = \frac{1}{K_{11}\{a_C\}} \qquad (13)$$

i.e. the activity of Si in the alloy phase is inversely proportional to the activity of C. This can be readily verified because $a_{Si} = \ddot{y}_{Si} X_{Si}$, where $\ddot{y}_{Si}$ is the activity coefficient of Si in the alloy as shown in Table II. The droplets shown in Fig. 10 have an Si concentration which is equivalent to $X_{Si} = 0.25$–0.27 and is significantly higher than a typical C-saturated blast-furnace liquid metal.

Thermodynamic conditions that would determine the unit activity of SiC can be established by considering the following equilibria:

$$(CO) = \{C\}_{Fe} + \tfrac{1}{2}(O_2) \qquad (14)$$

$\Delta G^0_{14} = 137\,508 + 43.7T$ J mol^{-1} CO.

$$(SiO) + \{C\}_{Fe} = [Si]_{Fe} + (CO) \qquad (15a)$$

$\Delta G^0_{15a} = 36\,385 - 37.4T$ J mol^{-1} CO.

$$(SiO) + 2\{C\}_{Fe} = \langle SiC\rangle + (CO) \qquad (15b)$$

$\Delta G^0_{15b} = -127\,415 + 88.3T$ J mol^{-1} CO.

By setting out the condition $a_0 = P_{O_2}^{1/2}$ in the range 10^{-5}–10^{-7} and $P_{CO} = 1$ atm in Equation 14 and $a_{SiC} = 1$ in Equation 11, the value of equilibrium constant can be evaluated for Equation 11. From these values the straight line relationships between $RT\ln K$ against T for univariants related to SiC formation have been plotted in Fig. 13. The nucleation of SiC

TABLE II (a) Dependence of Si and C activities in iron alloy upon O_2 and CO partial pressure at 1400 °C; Conditions: $P_{CO} = 1$ atm, $a_{SiC} = 1$.

Equilibria:			ΔG^0 $\Delta H^0 - T\Delta S^0$ (J)
$\{C\}_{Fe} + \frac{1}{2}O_2(g) = CO(g)$			$-137\,508 - 43.7T$
$SiO(g) + \{C\}_{Fe} = \{Si\}_{Fe} + CO(g)$			$36\,385 - 37.4T$
$SiO(g) + 2\{C\}_{Fe} = \langle SiC\rangle + CO(g)$			$-127\,415 + 88.3T$
$\{Si\}_{Fe} + \{C\}_{Fe} = \langle SiC\rangle$			$-13\,680 + 96.5T$
$a_0 = P_{O_2}^{\frac{1}{2}}$	$\{a_C\}$	P_{SiO}	$\{a_{Si}\}$
10^{-7}	2.653	0.649	10.01
10^{-6}	0.2653	64.96	100.1
10^{-5}	0.0265	6496	1001

(b) Activity coefficients of C and Si dissolved in liquid Fe at 1600 °C: $a_C = X_C\ddot{y}_C$; $a_{Si} = X_{Si}\ddot{y}_{Si}$

X_C	$\ddot{y}_C$	X_{Si}	$\ddot{y}_{Si}$
0.0	0.57	0.0	0.0013
0.05	0.85	0.1	0.003
0.10	1.37	0.2	0.009
0.15	2.30	0.3	0.04
0.20	4.12	0.4	0.178
		0.5	0.446

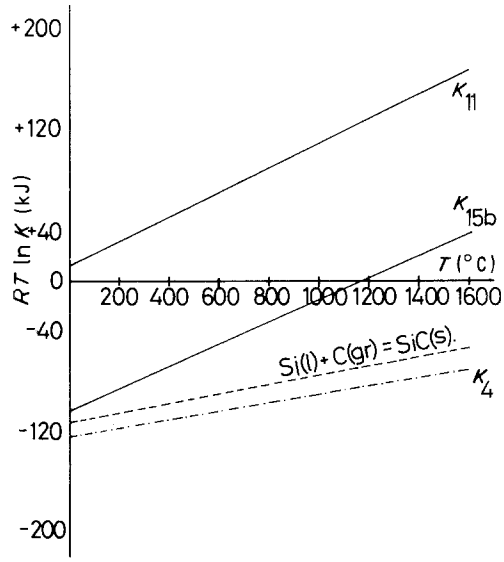

Figure 13 $RT\ln K_4$, $RT\ln K_{11}$ and $RT\ln K_{15b}$ versus T curves compared with the Si(l) + C(gr) = SiC(β) univariant. The equilibrium relationships indicate that the formation of β-SiC is more favourable as a_{Si} and a_C approach unity.

crystals is thermodynamically more favourable when activities of carbon and silicon are unity. In Table II the calculated values of $[a_C]$, $[a_{Si}]$ and P_{SiO} are summarized from which the inverse relationship between Si and C activity defined in Equation 13 is evident. Also included are the values of activity coefficients ($\ddot{y}_C$) for Si and C in liquid Fe at 1600 °C. Clearly the formation of SiC from the liquid Fe–Si–C alloy requires an extremely large activity of Si in the system (or a large P_{SiO}). However, under extremely reducing conditions as described earlier, a_{Si} values of the order of 10^3 during reduction of SiO gas makes Reaction 15a thermodynamically more feasible. It is also emphasized here that on the basis of reduction equilibria

calculation, it is apparent that there is a relatively smaller driving force for the nucleation of SiC via Reaction 11 than via Reaction 15b; the measure of driving force being $G_{SiC} = -RT \ln a_{SiC}$. This condition from Equation 12 also points out that at equilibrium, the activity of C in the alloy phase will be consequently lower than unity if β-SiC crystals are to form. No sooner does the alloy phase reach the critical activity values of silicon and carbon, than the SiC crystals nucleate. Hence the kinetics of mass transport of these two species in the alloy phase must compete with the nucleation and subsequent growth reactions of SiC.

3.6. The condition for interfacial tension between the alloy liquid Fe–Si–C and SiC

To understand the role of the interface between a solid phase and a liquid in equilibrium with a gas phase, it is important to invoke two different aspects of surface science. The first aspect deals with the dependence of interfacial tension, σ, on the activity or partial pressure of a species i at an isotherm. This relationship is called the Gibbs adsorption equation and is given below

$$\Gamma_i = -\frac{1}{RT} \cdot \frac{d\sigma}{d \ln a_i} \quad (16)$$

Here Γ_i is the relative adsorption or excess surface concentration of i. This equation is valid at a state of equilibrium condition and has been obtained from the free energy relation derived from the second law of thermodynamics. Evidently according to Equation 16, the adsorption of any species i causes a reduction in the surface tension.

The second aspect deals with the anisotropy of surface free energy in crystals. Owing to this, each crystallographic plane would be expected to have a different surface tension in equilibrium with a fluid phase. This is due to the Gibbs–Thompson effect according to which at a given thermodynamic activity or partial pressure of a species in the fluid phase, $\sigma(h_1 k_1 l_1) \neq \sigma(h_2 k_2 l_2)$ where $(h k l)$ defines the Miller indices of a plane.

When metallic silicon dissolves in Fe–C melts, the surface tension of the liquid decreases with increasing Si concentration [27]. For a dilute ternary solution of C and Si in liquid iron at 1600 °C, Belton [25] calculated the value of relative adsorption, Γ_{SiC}, by using Equation 16. This value in dilute solution range is 4.2×10^{-10} g mol cm^{-2} and it was pointed out that such a value of relative adsorption is too small for the formation of a surface compound having a close-packed hcp or fcc structure. Because SiC has a covalently bonded tetrahedron structure, a simple continuous plane with bonded atoms of Si and C is not possible. From so many atoms on the surface, the only possible topological arrangement will be weakly interacting chains of Si–C which is part of a three-dimensional crystalline structure.

Results from the carbothermic reduction of SiO discussed in previous sections have indicated that the formation of SiC whiskers is a function of P_{CO}, and also P_{SiO} required should be higher than the equilibrium value at a given temperature. This evidently implies that the Si content of liquid metal would be expected to vary with P_{CO}; consequently, the value of σ between the whiskers and metal droplets will be fixed by the value of a_{Si} in the Fe–Si–C liquid. The surface configuration of atoms of Si and C on the liquid alloy would therefore be strictly determined by the CO partial pressure imposed and this will result into a variation of the angle, θ, between the whiskers and metal droplets which are examined later.

Equilibrium calculations for the nucleation of SiC indicate that the activity of silicon in the melt has to be greater than unity (see Table II) at a given thermodynamic activity of O_2 (a_O). Such a thermodynamic condition would mean that the relative adsorption (cf. Equation 16 may demonstrate a non-linear behaviour at higher activities of silicon in the alloy because the activity composition relationship is not linear) may have to attain a much higher value for the nucleation of SiC. This implies that there would be an expected departure from the Henrian solution behaviour. For this thermodynamic reason it is not surprising that the crystals of SiC never form during cooling of either a blast-furnace hot metal or grey iron because these two are dilute solutions of Si in C-saturated liquid Fe. Clusters of close-packed topological structure would only form as a_{Si} rises; and only these atom assemblies would participate in the formation of SiC whiskers. We think that these close-packed surface clusters exist because the predominant whisker growth direction confirmed from TEM is ⟨1 1 1⟩ of fcc bravais lattice (see Section 3.7). In addition it is also pointed out from these surface thermodynamic properties that the topological configuration of atoms should continually change for such a causation, because the activity is a continuous function of composition in a solution.

Coleman and Sears [30] have derived, using a classical approach, a relationship between the value of supersaturation, α, required for nucleation of whiskers and the nucleation rate, N_0, which is related to the value of the interfacial energy, σ. This equation is given below where a is average atomic jump distance, M is the molecular weight, ρ and k are the density of the material and Boltzmann constant, respectively

$$\ln \alpha = \frac{\pi a \sigma^2 M}{\rho k R T^2} \cdot \frac{1}{\ln(B/N_0)} \quad (17)$$

An estimation of σ can be made by considering that the value of N_0 only depends upon σ for a given temperature, T, and α value. To evaluate N_0, Lee and Cutler [18] have given an expression for the percentage yield of SiC (%SiC) in the case of catalytic and non-catalytic reaction and this is given below

$$(\%\text{SiC}) = A\,(P_{CO})^{-1/3}\, t \exp\left(-\frac{\Delta\varepsilon}{RT}\right) \quad (18)$$

where A for an Fe catalysed reaction is 2.8×10^{10} (% (atm)$^{-\frac{1}{3}}$ min^{-1}) and this value rises to 4.25×10^{16} (% (atm)$^{-\frac{1}{3}}$ min^{-1}) for a non-catalytic reaction, whereas for these two conditions, Δε values are

335 and 545 kJ mol^{-1}, respectively. If it is assumed that the nucleation process also has a similar activation energy barrier, which may not be far from that of overall reduction process, then N_0 is related to the thermally activated barrier, $\Delta\varepsilon$, i.e.

$$N_0 \propto \exp\left(-\frac{\Delta\varepsilon}{RT}\right) \tag{19}$$

Equation 19, combined with isothermal and isochemical potential conditions, will yield

$$\left(\frac{\sigma_2}{\sigma_1}\right)^2 = \ln\left(\frac{N_{01}}{N_{02}}\right) \tag{20}$$

where suffixes 1 and 2 relate to the non-catalytic and catalytic reactions, respectively. This relationship at various temperatures is plotted in Fig. 14, where the ratio (σ_2/σ_1) varies linearly with temperature up to 1600 °C, but above this, there is a tendency for departure from linearity. The relationship given in Equation 20 thus yields the ratio $\sigma_2/\sigma_1 = 0.905$ which indicates that liquid ferrous alloy does have an effect on the nucleation process due to a reduction in interfacial tension. The contact angle, θ, (being a function of P_{CO}) between liquid alloy and whiskers produced at 1450 °C, shown in Fig. 10b for a "bead-necklace" morphology, varies between 127° and 133° indicating that the average $\cos\theta = \cos 130° = 0.907$ which is related to vapour–solid (σ_{sv}), vapour–liquid (σ_{lv}) and liquid–solid (σ_{ls}) interfacial energies, respectively, with the Young's equation [$= (\sigma_{sv} - \sigma_{ls})/\sigma_{lv}$].

3.7. Microstructural analysis using TEM

Whiskers produced by the reduction process were examined using 100 and 200 kV transmission electron microscopes. These whiskers were mounted on a copper grid which was soaked in a dilute mixture of a resin and acetone (1 : 10). The whiskers were spread on a clean sheet of paper and after the grids were dried, it had an adhesive tendency which allowed the mounting process to be possible without the introduction of any stress on the samples to be examined. This was particularly needed as the analysis of SADP is sensitive to stress accumulated in the sample.

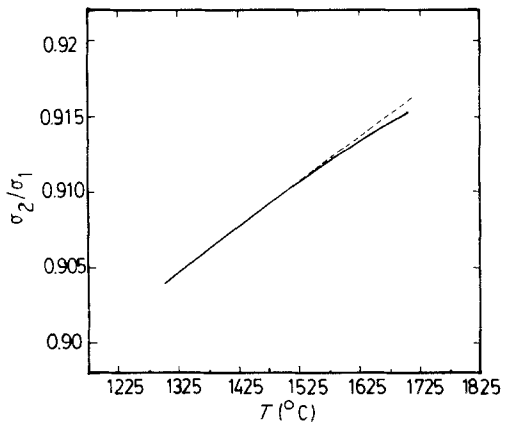

Figure 14 The interfacial tension ratio (σ_2/σ_1) versus T curve for the growth of β-SiC whiskers in the presence and absence of metallic Fe as catalyst.

Microstructural analysis of SiC using TEM has been extensively done in the past. The majority of workers have reported [16, 19, 20, 28, 31] that the whiskers produced under severely reducing conditions are of β-SiC and this was also verified using TEM. The polytype α-form has been reported by Mitchell and co-workers [7, 13, 14] to be more stable than β-SiC (3C type). In addition, they concluded from these investigations that the nucleation of the α-phase occurs at an incoherent twin boundary [14]. The stability of various kinds of polytypes and some aspects of their phase transformation have also been reported in this sequence of work by Mitchell and co-workers [7, 13, 14]. Of particular interest was the fact that the α-form is more stable under a higher O_2 partial pressure and is in agreement with other evidence in the literature [19, 20, 28]. Nutt [32] examined the microstructure of SiC produced from rice husks and proved that the impurities play a significant role in the nucleation of these whiskers. In this investigation, using high-resolution microscopy, the fine structure of SiC whiskers was studied and these were mostly characterized as microtwins. In the present investigation, the microstructure has been examined and the role of crystallographic defects (characterization to be discussed later) on the morphology and the growth process is explained below.

Two different types of whiskers were identified in this work; and these are shown in Figs 15 and 16. These are designated Type 1 and Type 2 whiskers. The selected-area diffraction pattern (SADP) (Fig. 16b) shows that the spots are streaked and in certain cases have satellites. These features confirm the presence of planar defects such as stacking faults (or "microtwins" as they are termed by a few authors [31, 32]). The diffraction pattern is analysed and has a [0 1 1] zone axis. The streaks on the diffracted spots are formed when S equals 0 and the streak direction thus indicates the corresponding habit plane; however, when $S \neq 0$, the Ewald sphere cuts the streaks at an angle thus forming satellites which appear in the SADP shown in Fig. 15c. The observation of streaks and satellites confirms the existence of a very high density of stacking faults. Fig. 15b is the dark-field image corresponding to the (1 1 1) spot. This image distinctly shows a contrast due to stacking faults which produce a phase shift; as a consequence dark and bright fringes form at the planar imperfection interface due to constructive and destructive interference between the transmitted and diffracted beam [33]. Van Torne [31] determined the size of microtwins which is of the order of 1.25 nm. In the SADP shown above, the (2 2 2) diffraction spot has a twin which is similar in nature to those identified by other authors [31, 32]. Here the whisker growth direction is ⟨1 1 1⟩. The size of microtwins appears to vary (see Fig. 15b) as indicated by the size of the dimension of the phase contrast band (marked in the figure). These are aperiodically spaced along the growth direction and each has a dimension of 0.25 nm which is one-fifth of the size of microtwins reported by Van Torne [31]. The SADP of Type 1 and Type 2 crystals (Fig. 16) also indicate that there is a considerable elastic strain accumulated in these

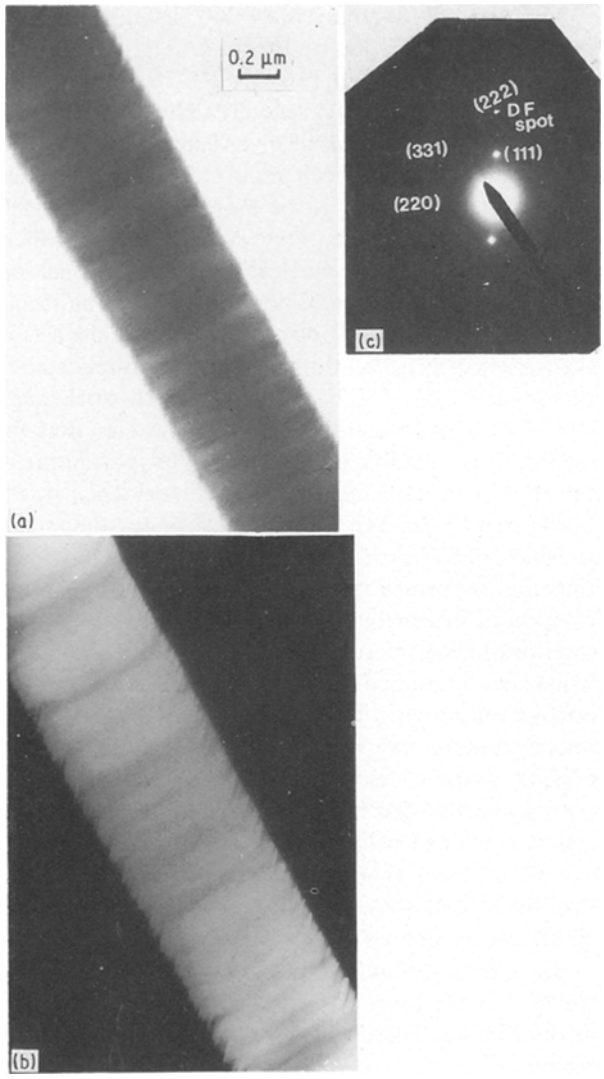

Figure 15 Transmission electron micrograph of a type 1 whisker. (a) Bright field, the inset is the SADP. (b) Dark field, (c) SADP.

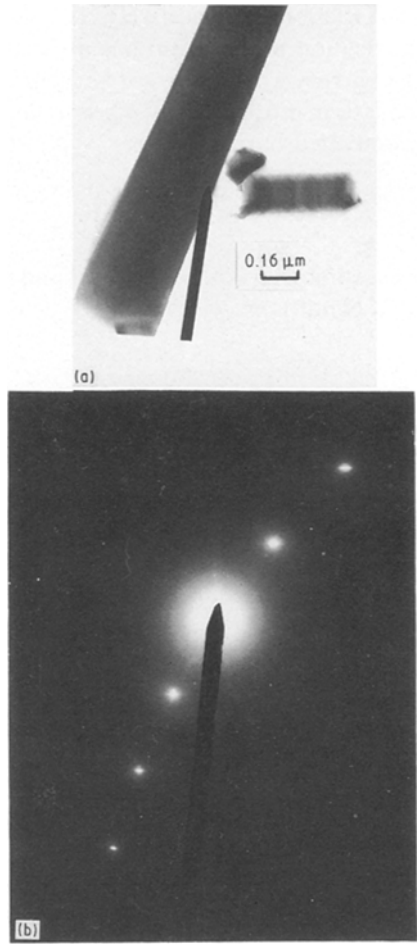

Figure 16 (a) Transmission electron micrograph of a type 2 whisker. (b) The SADP showing curvature of the spot pattern due to accumulated elastic strain during the growth process in the ⟨1 1 1⟩ direction.

whiskers. The curvature on the row of diffraction spots along the growth axis ⟨1 1 1⟩ demonstrates this. Such a diffraction pattern can also arise due to shape effects as pointed out by Hirsch *et al.* [34]; in the former case, the extension of the reciprocal lattice spots due to strain depends strongly on the indices of individual points, and is zero for the undiffracted beam. This extension, however, is constant when shape effects are encountered in the analysis of SADP. The microstructural features of Type 2 crystals are shown in Fig. 16 where the SADP has streaking but no satellites, thus indicating the condition $S = 0$ for diffraction. The bright-field image of whiskers does not show any contrast, unlike in the case discussed earlier (cf. Fig. 15a); which may point out that there may be whiskers in the bulk of the pellet which may not have developed any planar defects during the growth process.

3.8. Polytypism and the defect structure

The existence of α-SiC (hexagonal) polytypes is an unexplained observation and a great deal of uncertainty still exists as to their nature. Two features which can be concluded from this work and the published literature are

(i) the stability of α-SiC at higher oxygen potential;

(ii) the nucleation of α-SiC at incoherent twin boundaries.

What is apparent from the high-temperature processing of silicon carbide, is that if care is not exercised in controlling the concentration of oxygen in the gas phase necessary for $SiO(g) + 3CO(g)$ or $C(s) = SiC(s) + 2CO_2(g)$ or $CO(g)$ reaction, it is likely that oxygen may occupy some sites by replacing a few carbon atoms in the structure of β-SiC atoms. This may cause strain in the lattice due to the size difference between C and O atoms. Such strains are likely to be of an elastic nature. When this strain energy difference between a set of layers of Si and C arises, the incoherent twin boundary may form. Owing to this, it could be possible that the growing whiskers may not have a uniform distribution of crystallographic defects, which is to some extent apparent in Fig. 15b. This indicates that dislocations may appear due to this crystallographic misfit introduced by oxygen atom occupancy in the structure. The dark-field image in Fig. 15b shows the existence of hexagonal loops with denticulated surfaces resulting from the misalignment of corners of a hexagon. Each set of hexagonal loops, within which there is also some variation in the intensity, produces a maximum diffraction contrast only at

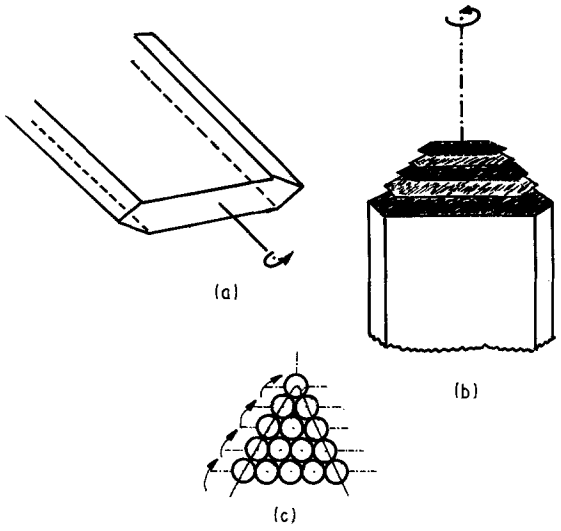

Figure 17 The schematic diagram of whisker growth. (a) No misorientation of growing ledge along the growth axis. (b) Misoriented ledges, (c) the tip of whiskers shown as layers of atoms.

a particular tilt angle, thus suggesting a multiplicity of orientation of (1 1 1) planes along the ⟨1 1 1⟩ growth direction. This is schematically shown in Fig. 17.

3.9. Growth mechanism

The multiplicity of orientation of hexagonal loops in Figs 15b and 17 points out that the growth process is perhaps assisted by a screw dislocation mechanism, where at the growth tip more than one dislocation could be present. Such a hypothesis is not too unreasonable if the stacking of Si–C layers is occurring in the presence of oxygen. Each screw dislocation thus formed is accompanied by a shear stress which in extreme case can produce a "twist" along the growth direction. This way accumulation of strain in the structure during growth process can occur. The value of the shear stress, τ, can be then expressed as $\tau = \boldsymbol{b}G/2\pi a(1 - \nu)$ where G is the shear modulus, a is the interatomic distance in the slip direction, $\boldsymbol{b}$ is the Burgers vector of a dislocation and ν is Poisson's ratio. If there is a twist along the length of each whisker the Eshelby model [35] proposes that the shearing of atoms will occur here, for example in the c-direction between two adjacent layers, and this in turn would determine the strength of these whiskers. If this is so, then the above equation for shear stress can mathematically define the value of τ. Petrovic *et al.* [36] measured the tensile properties of SiC whiskers and empirically showed that their strength is inversely proportional to their length. Eshelby's model is related to the twist angle, Ω, per unit length of whisker

$$\frac{\Omega}{L} = \frac{\boldsymbol{b}}{\pi r^2}\left(1 - \frac{\varepsilon'^2}{r^2}\right) \qquad (21)$$

where ε'/r is the displacement of the screw dislocation from the c-axis of a whisker. If $\varepsilon'/r = 0$, Ω (rad) varies with L/r which means the longer whiskers will suffer more angular twist and consequently their strength will decrease. The manifestation of strain during the growth process is a consequence of the screw dislocation growth mechanism which also offers a means for mass transport discussed elsewhere [37]. A screw dislocation, being a high chemical potential site, provides a mechanism for surface diffusion for both whiskers nucleating on Fe–Si and C (see Fig. 17c). The former is dictated by the transport of C and Si atoms from a liquid phase along the length of whiskers whereas the latter totally relies on deposition of Si and C atoms from the vapour phase via the $SiO(g) + 3CO(g) = SiC(g) + 2CO_2(g)$ reaction. Our experimental results, including those published in the literature [19, 28], support this argument and hence confirm the variation in the rate of growth under catalytic and non-catalytic reduction conditions.

Bootsma *et al.* [28] have determined that the activation energy for the growth process to be 320 kJ mol^{-1} and pointed out that this value is similar to the sum of enthalpies of various intermediate reactions. However, this value is three times smaller for the growth of SiC with soot as a reducting agent, as indicated in Sections 3.1 and 3.4. The thermally activated barrier for the growth of SiC in this particular process cannot be directly related to the enthalpy of reaction because had this been so, then there should not have been any difference in the values of activation energy of the reduction reactions, as several authors including Bootsma and co-workers point out. What is interesting from the comparison of E_a derived in this work and the value of activation energy for the growth of SiC (E_{gr}) with soot is that they are similar in magnitude which indicates that the growth of SiC whiskers in the presence of soot on lampblack is controlled by the rate of oxidation of a specific form of carbon.

4. Conclusions

SiC whiskers can be produced by carbothermic reduction of silica. At each CO partial pressure, the maximum rate of reduction was observed when precipitated Si was reduced with lampblack at 1650 °C. The activation energy for overall reduction process is 100 kJ mol^{-1} SiO_2 in the temperature range 1500–1650 °C. The reduction of SiO_2 at elevated temperatures follows Le Chatelier principle and hence the yield of SiC is determined by the imposed CO partial pressure. Under moderately low CO partial pressures, neither SiC powders nor whiskers were produced because of extremely high vapour pressure of SiO.

SiC whiskers were formed under those conditions when SiO and CO pressures were comparable for example at 1600 °C, if the imposed CO partial pressure was 0.25 atm, the SiO pressure was 0.23 atm. The whiskers produced were of β-SiC and electron microscopic examination indicated that these were faulted. These faults were predominantly due to the stacking of Si and C atoms in the ⟨1 1 1⟩ direction of fcc. Some whiskers also had accumulated elastic strain, as was indicated by the electron diffraction pattern.

The nucleation of whiskers occurred either on C particles or on the surface of the liquid Fe–Si–C alloy. The latter were frequently identified when Fe was used as catalyst during the reduction process. The

liquid Fe–Si–C alloy reduces the interfacial tension during the nucleation of SiC whiskers. The presence of denticulated hexagonal loops in the ⟨1 1 1⟩ growth direction of SiC whiskers indicated that the whiskers could be growing in the form of ledges.

Acknowledgements

The authors acknowledge the financial support from the Science and Engineering Research Council and the technical help received from Mr A. J. Reynolds, Experimental Technique Centre, Brunel University.

References

1. P. KRISHNA and A. R. VERMA, *Z. Kristallogr.* **121** (1965) 36.
2. A. R. VERMA and P. KRISHNA, in "Polymorphism and Polytypism in Crystals" (Wiley, New York, 1966) p. 13.
3. D. PANDEY and P. KRISHNA, in "Silicon Carbide 1973" (University of South Carolina Press, Columbia, SC, 1974) p. 198.
4. L. V. AZAROFF, in "Introduction to Solids" (Tata-McGraw-Hill, Bombay, 1977) p. 362.
5. W. HUME-ROTHERY and G. V. RAYNOR, in "The Structure of Metals and Alloys" (Institute of Metals, London, 1962) p. 186.
6. H. JAGODZIMSKI and H. ARNOLD, in "Silicon Carbide a High Temperature Semiconductor", Proceedings of the Conference on Silicon Carbide, Boston, MA, edited by J. R. O'Connor and J. Smittens (Pergamon Press, Oxford, 1960) p. 137.
7. A. E. HEUER, G. A. FRYBURG, L. U. OGBUJI and T. E. MITCHELL, *J. Amer. Ceram. Soc.* **61** (1976) 406.
8. T. E. MITCHELL, L. U. OGBUJI and A. H. HEUER, *ibid.* **61** (1976) 412.
9. S. SHINOZAKI and K. R. KINGMAN, *Acta Metall.* **26** (1978) 769.
10. N. SETAKA and K. EJIRI, *J. Amer. Ceram. Soc.* **52** (1969) 60.
11. S. AMELINCKX and G. STRUMANE, in "Silicon Carbide a High Temperature Semiconductor", Proceedings of the Conference on Silicon Carbide, Boston, MA, edited by J. R. O'Connor and J. Smittens (Pergamon Press, Oxford, 1960) p. 162.
12. J. G. ANTONOPOULOS, J. STOEMENOS, C. JAUSSAND and J. MARGAIL, *J. Mater. Sci. Lett.* **8** (1989) 1374.
13. L. U. OGBUJI, T. E. MITCHELL and A. H. HEUER, *J. Amer. Ceram. Soc.* **64** (1981) 91.
14. *Idem., ibid.* **64** (1981) 100.
15. K. OKAMURA, M. SATO, T. MATSUZAWA and Y. HASEGAWA, in "Ultrastructure Processing of Advanced Ceramics", edited by J. D. Mackenzie and D. R. Uhlrich (Wiley, New York, 1987) p. 501.
16. P. F. KNIPPENBERG, *Philips Res. Rep.* **18** (1963) 161.
17. STEVEN R. NUTT, *J. Amer. Ceram. Soc.* **71** (1988) 149.
18. J. G. LEE and I. B. CUTLER, *Ceram. Bull.* **54** (1975) 195.
19. J. V. MILEWSKI, F. D. GAC, J. J. PETROVIC and S. R. SKAGGS, *J. Mater. Sci.* **20** (1985) 1060.
20. H. WADA, M. J. WANG and T. Y. TIEN, *J. Amer. Ceram. Soc.* **71** (1988) 837.
21. E. T. TURKDOGAN and J. V. VINTERS, *Inst. Min. Metall. Trans. C* **85** (1976) 117.
22. P. L. WALKER Jr, M. SHELF and R. A. ANDERSON, in "Chemistry and Physics of Carbon", Vol. 4, edited by P. L. Walker Jr (Edward Arnold, London, 1968) p. 317.
23. E. T. TURKDOGAN and J. V. VINTERS, *Carbon* **7** (1969) 101.
24. *Idem., ibid.* **10** (1972) 97.
25. G. R. BELTON, *Met. Trans.* **3** (1972) 1465.
26. D. POHL and E. SCHEIL, *Giesserei* **43** (1956) 833.
27. T. J. WHALEN, S. M. KAUFMAN and M. HAMENIK Jr, *Trans ASM* **55** (1962) 779.
28. G. A. BOOTSMA, W. F. KNIPPENBERG and G. VERSPIPI, *J. Crystal. Growth* **11** (1971) 297.
29. J. R. O'CONNOR and J. SMITTENS (eds), "Silicon Carbide a High Temperature Semiconductor", Proceedings of the Conference on Silicon Carbide, Boston, MA (Pergamon Press, Oxford, 1960) p. 25.
30. R. V. COLEMAN and G. W. SEARS, *Acta Metall.* **5** (1957) 131.
31. L. I. van TORNE, *J. Appl. Phys.* **37** (1966) 1849.
32. S. R. NUTT, *J. Amer. Ceram. Soc.* **71** (1988) 149.
33. S. AMELINEX, in "Direct Observation of Dislocation" (Academic Press, New York, 1964) p. 139.
34. P. B. HIRSCH, A. HOWIE, R. B. NICHOLSON, D. W. PASHLEY and M. J. WHELAN, in "Electron Microscopy of Thin Crystals" (Krieger, Malabar, FL, 1977) p. 130.
35. J. D. ESHELBY, *J. Appl. Phys.* **24** (1952) 176.
36. J. J. PETROVIC, J. V. MILEWSKI, D. L. ROHR and F. D. GRAC, *J. Mater. Sci.* **20** (1985) 1167.
37. A. JHA and P. GRIEVESON, *ibid.* **25** (1990) 2299.

Received 5 November
and accepted 19 November 1990